https://doi.org/10.5194/mr-2023-8
Preprint. Discussion started: 22 May 2023


Open Access MAGNETIC RESONANCE Discussions



# Monte-Carlo Analysis of Asymmetry in Three-Site Relaxation Exchange: Probing Detailed Balance

Bernhard Blümich,[1] Matthew Parziale,[2] and Matthew Augustine[2]

[1] Institut für Technische und Makromolekulare Chemie, RWTH Aachen University, Worringer Weg 2, 52074 Aachen, Germany

[2] Department of Chemistry, UC Davis, One Shields Avenue, Davis, CA 95616, USA

Corresponding author: Bernhard Blümich, bluemich@itmc.rwth-aachen.de

The question is investigated if three-site diffusive relaxation exchange in thermodynamic equilibrium can lead to exchange maps, which are asymmetric for fluids confined to pores. Asymmetry reports circular flow of particles between the relaxation sites which disagrees with detailed balance according to which the particle exchange between any pair of sites must be balanced. Vacancy diffusion and gas diffusion of particles confined to two-dimensional pores were modeled in Monte-Carlo simulations. For each particle move in vacancy diffusion on a 2D checkerboard grid, one of the eight neighboring destination cells was identified on the basis the jump probability calculated from an empirical approximation of the free energy. Gas diffusion was simulated without thermodynamic interaction on a simulation grid which was up to $10^4$ times finer than the particle diameter. It was found that up to 1% of all particles moves coherently in closed paths. This motion is attributed to pore resonance corresponding to diffusion eigenmodes. The study shows that detailed balance of multi-site exchange does not apply for a small fraction of particles when the exchange is impacted by topological constraints.

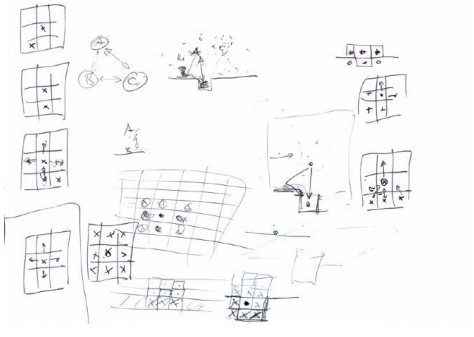

Graphical abstract: Draft of particle exchange on a 2D checkerboard grid

https://doi.org/10.5194/mr-2023-8
Preprint. Discussion started: 22 May 2023


Open Access MAGNETIC RESONANCE Discussions



## 1. Introduction

Exchange phenomena are an essential ingredient of diffusion and spreading phenomena, which are abundant in nature and govern the evolution of tangible and intangible objects and goods (Bunde et al., 2018). Nuclear Magnetic Resonance provides particularly powerful methodologies to investigate molecular exchange processes (Ernst et al., 1987; Callaghan, 2011). Slow molecular exchange on the millisecond time scale is studied by two-dimensional exchange NMR, i. e. by chemical exchange spectroscopy for rotational motion (Jeener et al., 1979) and by exchange relaxometry for translational motion (Lee et al., 1993). In equilibrium the nature of the exchange processes is commonly understood to be random Brownian motion, and the 2D exchange maps are expected to be symmetric with respect to their diagonal. On the other hand, exchange in non-equilibrium leads to asymmetry in 2D NMR maps. This has been observed, for example, in 2D chemical exchange spectra for chemical reactions involving different sites (Lacabanne et al., 2022), for the spread of hyperpolarization by spin diffusion (Björgvinsdóttir et al., 2021), and for slow flow across porous media in relaxation exchange maps (Olaru et al., 2012).

The kinetics of transitions or exchange between discrete states driven by random processes are described by (van Kampen, 1992)

$$\frac{\mathrm{d}M_i(t)}{\mathrm{d}t} = \sum_j \{k_{ij}M_j(t) - k_{ji}M_i(t)\}, \tag{1}$$

where $M_i$ are populations or longitudinal magnetization components collected in the vector $\boldsymbol{M}$, and $k_{ij}$ are the exchange rates equivalent to the transition probabilities from state *j* to state *i*, which are collected in the kinetic exchange matrix $\mathbf{k}$. In equilibrium

$$\frac{\mathrm{d}M_i(t)}{\mathrm{d}t} = 0, \tag{2}$$

and the number of all particles arriving at site *i* from sites *j* is equal to the number of all particles leaving from site *i* to sites *j* so that the total mass is conserved.

As a result of mass balance, two-site exchange between states or sites A and B always leads to symmetric 2D NMR exchange maps in thermodynamic equilibrium as the number $k_{\mathrm{BA}}M_{\mathrm{A}}$ of particles populating site B by leaving site A per unit time is equal to the number of particles $k_{\mathrm{AB}}M_{\mathrm{B}}$ leaving site B and populating site A per unit of time. This number is the product of the rate $k_{\mathrm{BA}}$ for transitions from site A to site B times the population $M_{\mathrm{A}}$ of site A. The relationship $k_{\mathrm{BA}}M_{\mathrm{A}} = k_{\mathrm{AB}}M_{\mathrm{B}}$ is known as the 'principle of detailed balance'. It is usually taken to also apply to rate processes involving more than two sites.

https://doi.org/10.5194/mr-2023-8
Preprint. Discussion started: 22 May 2023


Open Access MAGNETIC RESONANCE Discussions



By example of mass-balanced equilibrium diffusion between three sites (Sanstrom, 1983), eqn. (1) becomes

$$\begin{aligned} k_{21}M_1 + k_{31}M_1 &= k_{12}M_2 + k_{13}M_3, \\ k_{12}M_2 + k_{32}M_2 &= k_{21}M_1 + k_{23}M_3, \\ k_{13}M_3 + k_{23}M_3 &= k_{31}M_1 + k_{32}M_2, \end{aligned} \tag{3}$$

or equivalently, mass balance requires

$$k_{12}M_2 - k_{21}M_1 = k_{31}M_1 - k_{13}M_3 = k_{23}M_3 - k_{32}M_2. \tag{4}$$

Normalization of this expression to the total number of exchanges per unit time defines the asymmetry parameter $a_{\mathrm{sy}}$ to be used below,

$$(k_{23}M_3 - k_{32}M_2)/[(1 \quad 1 \quad 1)\,\mathbf{k}\,\boldsymbol{M}] \stackrel{\text{def}}{=} a_{\mathrm{sy}}. \tag{5}$$

While mass balance (4) is a necessary condition for dynamic equilibrium, detailed balance, on the other hand, is a stronger condition and requires

$$a_{\mathrm{sy}} = 0. \tag{6}$$

Detailed balance had been introduced by Maxwell in 1867 based on ‘sufficient reason’ in his derivation of the speed distribution of gas atoms considering the speed exchange between colliding gas atoms in thermodynamic equilibrium (Maxwell, 1867). An intriguing consequence of the exchange being balanced in detail between particles A and B amounts to the impossibility of assigning positive time to either velocity exchange from A to B or B to A on the particle scale of the exchange process, thus admitting negative time or time reversal. In 1872 Boltzmann showed in an elaborate treatment, that Maxwell’s speed distribution also applies to polyatomic gas molecules (Boltzmann, 1872). Furthermore, in 1917 Einstein derived Planck’s law of black-body radiation as a balanced energy exchange between quantized radiation and matter underlining the striking similarity to Maxwell’s speed distribution of gas atoms (Einstein, 1917). He concludes “Indem Energie und Impuls aufs engste miteinander verknüpft sind, kann deshalb eine Theorie erst dann als berechtigt angesehen werden, wenn gezeigt ist, daß die nach ihr von der Strahlung auf die Materie übertragenen Impulse zu solchen Bewegungen führen, wie sie die Wärmetheorie verlangt,” (Since energy and momentum are intimately connected, a theory can only then be considered justified, when it has been shown, that according to it the momenta of the radiation transferred to the matter lead to such motions as demanded by the theory of heat.)

In his work extending Maxwell’s speed distribution to polyatomic gas molecules Boltzmann considered molecules in a container whereby the walls reflect the molecules like elastic balls: “Bezüglich der Gefäßwände, welche das Gas

https://doi.org/10.5194/mr-2023-8
Preprint. Discussion started: 22 May 2023


Open Access MAGNETIC RESONANCE Discussions



umschließen, will ich jedoch voraussetzen, dass die Moleküle an denselben wie elastische Kugeln reflektiert werden. … Die Wände stören nicht, da an ihnen die Moleküle wie elastische Kugeln reflektiert werden; also geradeso von ihnen zurücktreten, als ob der Raum jenseits der Wände von gleich beschaffenem Gase erfüllt wäre.“ (Concerning the container walls which enclose the gas, I want to presume that the molecules are reflected from them like elastic balls. …. The walls do not interfere, because the molecules are reflected from them like elastic balls; that is, recede from them just like that, as if the space beyond the walls would be filled with similarly conditioned gas.) Moreover, the interaction between gas molecules can be of any type. While he claimed that any other interaction between walls and molecules would lead to the same result albeit at loss of simplicity, the perfectly elastic reflections of the gas molecules at the walls would eliminate the topological constraints of the box on their motion. Boltzmann obtained the same speed distribution for polyatomic molecules with internal degrees of freedom as Maxwell had for atoms based on detailed balance of speed exchange. In the simulations reported below, the motion of molecules is considered for which the interactions with the walls are the same as those among the molecules. Understanding confined diffusion (Valiullin, 2017) is important from a general point of view because the motion of molecules without topological constraints is an ideal limit which cannot perfectly be realized in practice although it may be realized within experimental uncertainty.

Two-site exchange processes will always be symmetric in thermodynamic equilibrium. This situation has been evaluated analytically for NMR relaxation exchange of fluids in porous media (McDonald, 2005). Yet multi-site relaxation-exchange NMR maps (Van Landeghem, 2010) can from a mathematical point of view be asymmetric. For example, the transverse magnetization $s(t_1, t_2)$ from a three-site $T_2$-$T_2$ relaxation exchange NMR experiment (Gao and Blümich, 2020),

$$s(t_1, t_2) = (1,1,1)e^{-(\mathbf{R}_2+\mathbf{k})t_2}e^{-(\mathbf{R}_1+\mathbf{k})t_\mathrm{m}}e^{-(\mathbf{R}_2+\mathbf{k})t_1}\boldsymbol{M}(t_0), \quad (7)$$

has been simulated to model an experimentally observed asymmetric three-site $T_2$-$T_2$ NMR exchange map of water molecules saturating $Al_2O_3$ powder with the three relaxation sites corresponding to bulk water, water molecules on the surface of the powder particles and water molecules inside the surface pores (Fig. 1). Here $\boldsymbol{M}(t_0)$ is the initial vector of transverse magnetization components from relaxation sites 1, 2 and 3 generated from longitudinal thermodynamic equilibrium magnetization with a 90° pulse at the beginning of the experiment at time $t_0$, and $t_1$, $t_\mathrm{m}$, $t_2$ are the evolution,

https://doi.org/10.5194/mr-2023-8
Preprint. Discussion started: 22 May 2023


Open Access MAGNETIC RESONANCE Discussions



mixing, and detection time intervals of the 2D NMR experiment, respectively (Callaghan, 2011; Lee et al., 1993). Apart from the relaxation-rate matrices $\mathbf{R}_1$ and $\mathbf{R}_2$, and the kinetic matrix $\mathbf{k}$, the best match obtained by forward simulation returned the peak integrals revealing an asymmetry parameter of $a_{\mathrm{sy}} = -1.2\%$. This asymmetry of the forward and backward particle jumps between two sites specifies the percentage of circular exchange events per unit time between the three sites in thermodynamic equilibrium (Fig. 1).

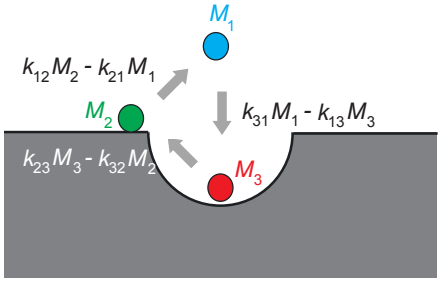


Figure 1. Asymmetry in three-site diffusion-mediated exchange indicates coherent circular motion by example of water molecules in contact with porous $Al_2O_3$ grains. Three water populations $M_j$ are identified by different NMR relaxation times and color. They are molecules in the bulk (1), molecules on the particle surface (2) and molecules in the pores (3). The exchange rate constants are $k_{ji}$. The net particle flux between two sites differs from zero. The net mass of all molecules participating in the exchange is conserved. The figure illustrates positive $a_{\mathrm{sy}}$.

While it can be argued that the experimental value of asymmetry lies within the measurement uncertainty, molecular dynamics simulations are reported and discussed below to investigate whether asymmetry in three-site exchange is just a mathematical peculiarity or a realistic physical phenomenon. This study is thought provoking in view of the fact, that asymmetric three-site exchange disagrees with detailed balance of the exchange between any pair of sites and needs to be explained by circular diffusion on the pore scale in thermodynamic equilibrium. Such motion resembles that of a rachet which Feynman has argued to disagree with the second law of thermodynamics (Feynman et al., 1966).

## 2. Modelling confined diffusion

### 2.1 Vacancy diffusion: Random particle jumps on a 2D checkerboard

Random jumps of particles from occupied sites to vacant sites were simulated with a Monte-Carlo algorithm (Grebenkov, 2011; Hughes, 1995; Sabelfeld, 1991) in a

https://doi.org/10.5194/mr-2023-8
Preprint. Discussion started: 22 May 2023


Open Access MAGNETIC RESONANCE Discussions



161 confined space on a checkerboard. The algorithm models vacancy diffusion (Seitz,
162 1948) encountered in metals and alloys but the particles perform the jumps rather than
163 the vacancies. To keep the simulation simple, it is limited to jumps on a 2D 3×3 Moore
164 lattice of range 1 (Wolf-Gladrow, 2000) following rules of the game of life (Wolf-
165 Gladrow, 2000; Bialnicki-Birula, 2004). Here the center particle can jump to any of its
166 8 neighbors. Different neighborhoods of range 1 were tested (Fig. S1) (Bialnicki-Birula,
167 2004), but only the Moore neighborhood having the highest symmetry of all
168 neighborhoods, produced data consistent with Eqn. (4). Topological constraints are
169 introduced which set boundaries to the jump space. Initially, the available cells inside
170 the jump space on the grid are populated randomly with particles up to a specified
171 particle density. Particles in the bulk are indexed 1, and two distinct boundary sections
172 are indexed 2 and 3, giving three environments between which randomly selected
173 particles can move. A particle jumping from environment *j* to *i* is counted by
174 incrementing the element *ij* of a 3×3 jump matrix by 1. If the particle environment does
175 not change with the jump, the respective diagonal element is incremented.
176

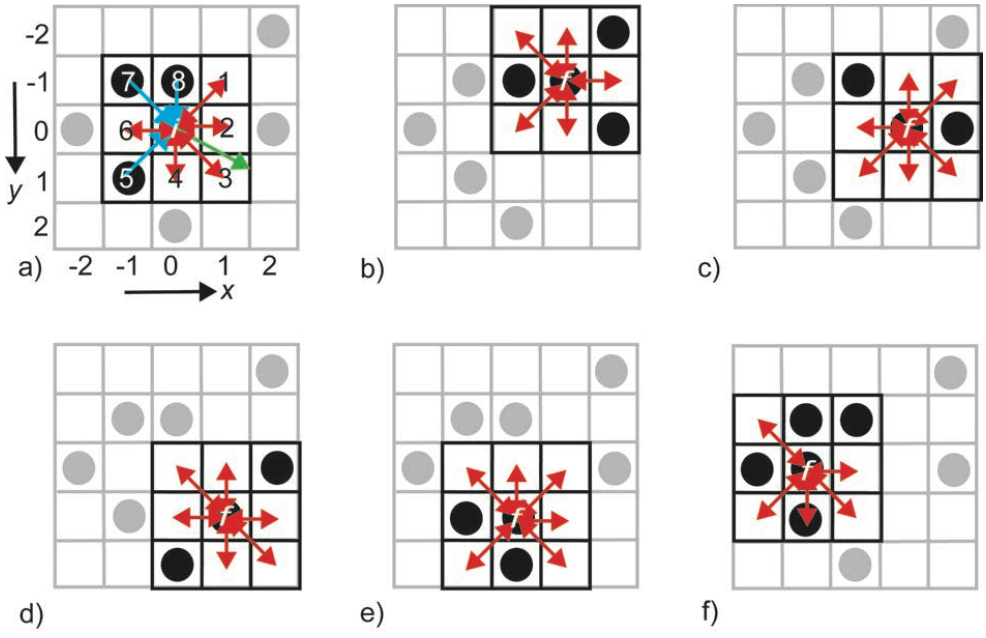


177
178 Figure 2. Checkerboard randomly occupied by particles represented by filled circles.
179 a) The cells surrounding the initial particle position *i* are numbered clockwise from 1 to
180 8. Cells 5,7, and 8 are occupied, the others are empty. The force (green arrow) on the
181 center particle is calculated as the sum of forces exerted from all particles in the
182 occupied nearest neighbor cells (blue arrows). The entropy is estimated from the sum

https://doi.org/10.5194/mr-2023-8
Preprint. Discussion started: 22 May 2023


Open Access MAGNETIC RESONANCE Discussions



of distances to all neighboring free cells (red double arrows). b-f) The center particle in a) can jump to any of the free cells 1, 2, 3, 4, and 6, each of which has its own entropy. The final position *f* of the jump is identified by evaluating the jump probability based on a simple heuristic model of the free jump-energy difference.

A particle on a square grid has eight nearest neighbor cells to which it can jump. (Fig. 2a). If more than one out of all neighbor cells are empty and thus available as destination cells for the jump, the destination cell is identified by evaluating the jump probability for each destination cell based on a simple heuristic model of the free jump-energy difference (Fig. 2b-f). At constant temperature and constant volume, the particle motion is governed by the Helmholtz free energy $A = U - T\,S$, where $U$ is internal energy, $T$ is temperature, and $S$ is entropy. In thermodynamic equilibrium, $A$ is at its minimum. The probability of a particle moving from one cell to another is given by the Boltzmann distribution $p = \exp\left\{-\frac{\Delta A}{k_B T}\right\}$, where $\Delta A = \Delta U - T\,\Delta S$.

The free energy change $\Delta A = \Delta U - T\,\Delta S$ is determined from crude models of the internal energy change $\Delta U = \boldsymbol{F}\,\Delta\boldsymbol{R}$ defined by the repulsive net force $\boldsymbol{F}$ exerted from all neighboring particles on the particle at stake and the length $|\Delta\boldsymbol{R}|$ of the jump to the next cell, the temperature $T$, and the entropy change $\Delta S$. The force $\boldsymbol{F}$ between two particles follows Newton's inverse square distance law. It is proportional to $\frac{1}{|\Delta\boldsymbol{R}|^2}$ in the direction of $\frac{1}{|\Delta\boldsymbol{R}|}\Delta\boldsymbol{R}$ from an occupied cell *j* to the particle *i* under consideration. The total force the particle *i* experiences is the vector sum of the forces exerted from the particles *j* in all occupied neighbor cells (Fig. 2a),

$$\boldsymbol{F}_i = \sum_j \frac{1}{|\Delta\boldsymbol{s}_{j,i}|^3}\Delta\boldsymbol{R}_{j,i}. \quad (8)$$

The internal energy change $\Delta U_{f,i}$ is computed for each potential jump from the initial occupied cell *i* to the final empty cell *f* by the product of the net force $\boldsymbol{F}_i$ with the vector $\Delta\boldsymbol{R}_{f,i}$ connecting the centers of the initial cell *i* and the final cell *f*.

The entropy change $\Delta S = S_f - S_i$ is the difference between the entropies of the particle with its eight nearest neighbors for the final state *f* and the initial state *i*. It is estimated by the sum of the step lengths $R_{f,i} = |\Delta\boldsymbol{R}_{f,i}|$ of the particle *i* to its unoccupied next nearest neighbor cells *f*,

$$S_i = \sum_f \Delta R_{f,i}. \quad (9)$$

In case a neighbor cell is occupied, $\Delta\boldsymbol{R}_{f,i} = 0$. Detailed examples are worked out in the supplementary information (Fig. S2).

https://doi.org/10.5194/mr-2023-8
Preprint. Discussion started: 22 May 2023


Open Access MAGNETIC RESONANCE Discussions



With these definitions jump probabilities $p = \exp\left\{-\frac{\Delta A}{k_B T}\right\}$ can be calculated. In each jump step, an initially occupied cell *i* is selected at random and $p$ is evaluated for all possible jumps to neighboring empty cells as potential final cells *f*. If for one or more jumps $p \geq 1$, the destination cell of the jump is picked at random from this subset of all potential jumps. If all neighbor cells are occupied, $p = 0$, and no jump is possible. If $0 < p < 1$ the destination cell is chosen at random from all those with the same largest jump probability $p < 1$.

In the simulations reported below, the Boltzmann constant $k_\mathrm{B}$ has been set to 1 and so has the shortest distance between neighboring cells. Depending on the type of cell, periodic boundary conditions (Fig. 3a) or rigid boundaries (Fig. 3b) were employed. A cell boundary has been treated just like an occupied cell with the same definition of the free energy in the calculation of the jump probability.

The simulations were carried out with a program written in Matlab R2020a by The MathWorks Inc. on an Apple MacBook Pro 2.4 GHz having an Intel Quad-Core i5 processor. Typically, $10^7$ jumps were simulated in one run taking 75 seconds.

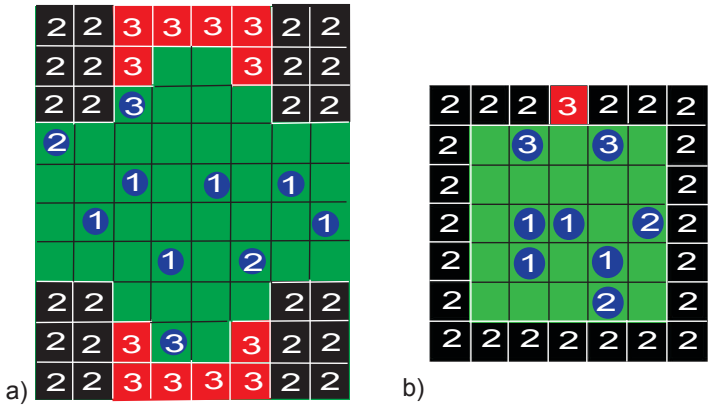


Figure 3. Examples of pore models for two-dimensional three-site exchange based on a checkerboard grid. Particles can occupy one cell and jump to a neighboring empty one based on the free-energy difference of the jump. a) Porous solid. The boundaries right and left are periodic. The boundaries top and bottom are rigid. Depending on their next neighbors in the first coordination shell, the particle-relaxation environments are identified as bulk (1), surface (2) or pore (3). b) Small square pore with an active site. The bulk (1), the walls (2), and the active site (3) have different relaxation properties. If a particle cell contacts two different relaxation sites, the higher number overrides the lower number when identifying its relaxation environment.

https://doi.org/10.5194/mr-2023-8
Preprint. Discussion started: 22 May 2023


Open Access MAGNETIC RESONANCE Discussions



### 2.2 Gas diffusion

The gas diffusion calculations explore similar pore size and occupancy. Here the motion of circular particles with diameter equal to the cell size was accomplished by propagating an initial Maxwell–Boltzmann distribution of particle speeds for random initial positions in a Monte Carlo fashion based on instantaneous collisional forces. The collisions change both the direction and velocity of the particles at each of the $10^9$ constant time increments used here. These elastic collisions with other particles and the wall are mediated by the particle size, which is set to be a fraction of the pore side length of one. This means that a square pore with a five-particle diameter side length is populated with particles having a diameter of 1/5. To compare the continuous positional output of this model to vacancy diffusion, a two-dimensional square grid with cell size set by the particle diameter is imposed on the entire pore. The quasi-continuous positional output is then binned into these cells and compared to the binned positions from the previous observation to determine if particles translated between the main pore volume, pore wall, and active site. The translational information is used to assign estimates of the jump-matrix elements and thus the asymmetry parameter $a_{\mathrm{sy}}$. The distribution of particles in the pore is recorded at constant time intervals, whereas for vacancy diffusion it is recorded after each jump.

## 3. Results

Two different pore geometries were analyzed. Initially the simulation was executed for a pore geometry (Fig. 3a) which approximates the pore structure of Fig. 1 and which is hypothesized to explain the observed asymmetry of water diffusing in a porous $Al_2O_3$ grain pack (Gao and Blümich, 2020). It is mirrored vertically to double the probability of particles entering the dent (relaxation site 3) in the otherwise straight surface (relaxation site 2). The bulk of the particles defines relaxation site 1. This complex pore structure was studied first, and the simulations revealed the existence of asymmetric exchange. To understand the essence of the asymmetry a simple square pore with an active site was studied in detail modelling confined diffusion in a small pore. The bulk, the walls and the active site have different relaxation properties (Fig. 3b). For both structures, the asymmetry parameter $a_{\mathrm{sy}}$ was evaluated for vacancy diffusion as a function of temperature and pressure. The results for the complex pore a reported in the supplementary material, whereas those for the simple square pore are reported in the main text here. Pressure was varied in terms of the population density measured

https://doi.org/10.5194/mr-2023-8
Preprint. Discussion started: 22 May 2023


Open Access MAGNETIC RESONANCE Discussions



277 as the fraction of cells occupied in the pore. At certain temperatures and pressures
278 also the autocorrelation function of the occupation-time track of a particular cell and its
279 Fourier transform were determined. Striking features observed in vacancy diffusion
280 were subsequently modelled for gas diffusion in the square pore.

281 Relevant results for the square pore (Fig. 3b) are summarized in six graphs in
282 Fig. 4. The asymmetry parameter varies strongly with temperature $T$ (Figs. 4a,b) and
283 pressure corresponding to population density $P$ (Figs. 4e,f). All parameters are relative
284 quantities without units. The top three graphs a), b) and c) show the variation of $a_{\mathrm{sy}}$
285 with temperature for a population fraction of 0.3 corresponding that of a gas. The
286 asymmetry parameter assumes only negative values in an abrupt but reproducible
287 manner in the range of -0.8% < $a_{\mathrm{sy}}$ < 0.0% for repulsive interaction (Fig. 4a), i. e. for
288 the definition of the force between particles as illustrated in Fig. 2a. With reference to
289 Fig. 1, negative $a_{\mathrm{sy}}$ reports that the straight exit route from the active site towards the
290 center of the pore is preferred over the detour via the pore wall. When the interaction
291 is changed from repulsive to attractive by inverting the sign of $\Delta U$ in the expression for
292 the free energy, the asymmetry parameter varies as well, however, only between -
293 0.3% < $a_{\mathrm{sy}}$ < 0.0% (Fig. 4b). In either case, the asymmetry parameter varies with the
294 thermodynamic conditions. It is concluded, that for this small pore, up to about 1% of
295 all jumps on the checkerboard can proceed in an ordered circular fashion between the
296 three sites. Similar behavior is observed for the complex pore of Fig. 3a as illustrated
297 in Fig. S3 in the supplement.

298 At the extrema of the $a_{\mathrm{sy}}(T)$ curves in Figs. 4a,b the dependence of the
299 asymmetry parameters on population density was investigated (Figs. 4d-f). The
300 variations with population density are smoother than those with temperature.
301 Significant negative asymmetry results at intermediate pressure, while at low and high
302 pressure, the asymmetry is small (Fig. 4d,e). At higher temperature and high pressure,
303 small positive $a_{\mathrm{sy}}$ is observed (Fig. 4d, $T$ = 0.8, $P$ = 0.8). If the interaction between
304 particles and walls is turned off, i. e. $\Delta A = 0$, essentially noise more than two orders of
305 magnitude smaller than with particle interaction is observed for the exchange
306 asymmetry determined from $10^6$ jumps when varying $T$ and $P$, however, with a small
307 bias towards negative $a_{\mathrm{sy}}$ (Figs. 4c,f). This suggests that the non-zero values for $a_{\mathrm{sy}}$
308 reported in Figs. 4a,b,d,e are trustworthy.
309

https://doi.org/10.5194/mr-2023-8
Preprint. Discussion started: 22 May 2023


Open Access MAGNETIC RESONANCE Discussions



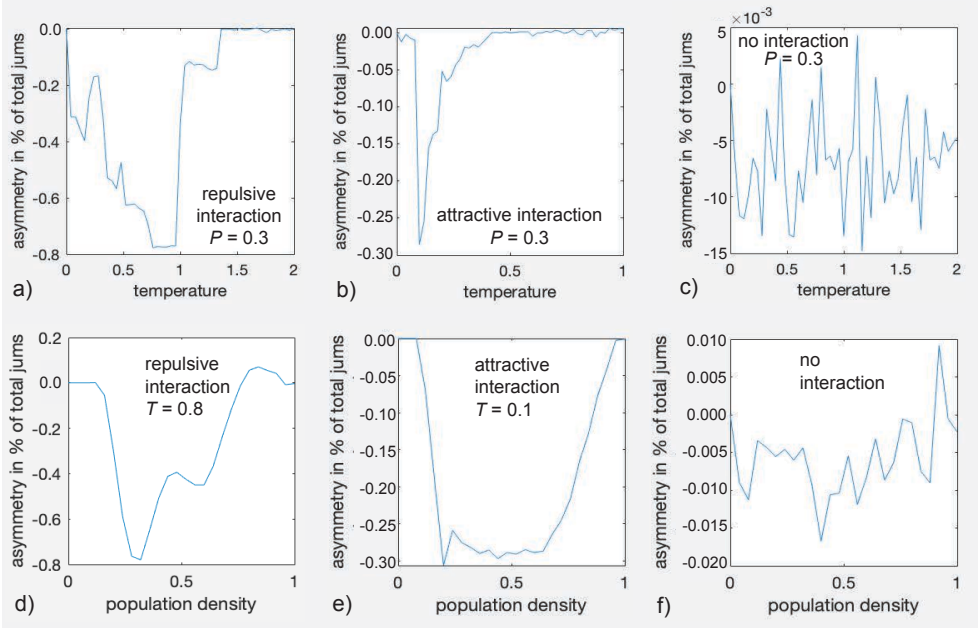


Figure 4. Asymmetry parameters $a_{sy}$ for diffusion inside the small rectangular pore depicted in Fig. 3b as a function of temperature $T$ (a-c) and pressure $P$ (d-f). a) $a_{sy}(T)$ for repulsive interaction at $P = 0.3$. b) $a_{sy}(T)$ for attractive interaction at $P = 0.3$. c) $a_{sy}(T)$ without interaction. d) $a_{sy}(P)$ for attractive interaction at $T = 0.8$. e) $a_{sy}(P)$ for attractive interaction at $T = 0.1$. f) $a_{sy}(P)$ without interaction.

To shed further light on the origin of the asymmetry, autocorrelation functions of the occupation-time tracks of selected cells in the pore were computed and Fourier transformed (Fig. 5). The occupation-time track was calibrated to zero mean for purely random occupation, i. e. it contained the negative population density when it was empty and the complement of the population density to one when the cell was occupied. The faster the autocorrelation function decays, the less coherent the cell population fluctuates and the broader is its Fourier transform, i. e. the transfer function (Fig. 5b,c). A constant offset of the autocorrelation function shows that the time-average population in the cell differs from the mean population of the pore (Fig. 5a,b). This offset produces a spike at zero frequency in the transfer functions. Subtracting the offsets from the autocorrelation functions and scaling the resulting functions to the same amplitude reveals different decays in different cells and thus variations in particle dynamics across the pore (inset in Fig. 5c, middle). These dynamics cannot readily be measured for a single cell in the pore, although an average over all cells and pores in the measurement volume would be amenable to experiment by probing the particle

https://doi.org/10.5194/mr-2023-8
Preprint. Discussion started: 22 May 2023


Open Access MAGNETIC RESONANCE Discussions



dynamics with CPMG measurements in magnetic field gradients at variable echo time. Such measurements provide the frequency-dependent diffusion coefficient as the Fourier transform of the velocity autocorrelation function (Stepišnik et al., 2014, Callaghan and Stepišnik, 1995; Parsons et al., 2006).

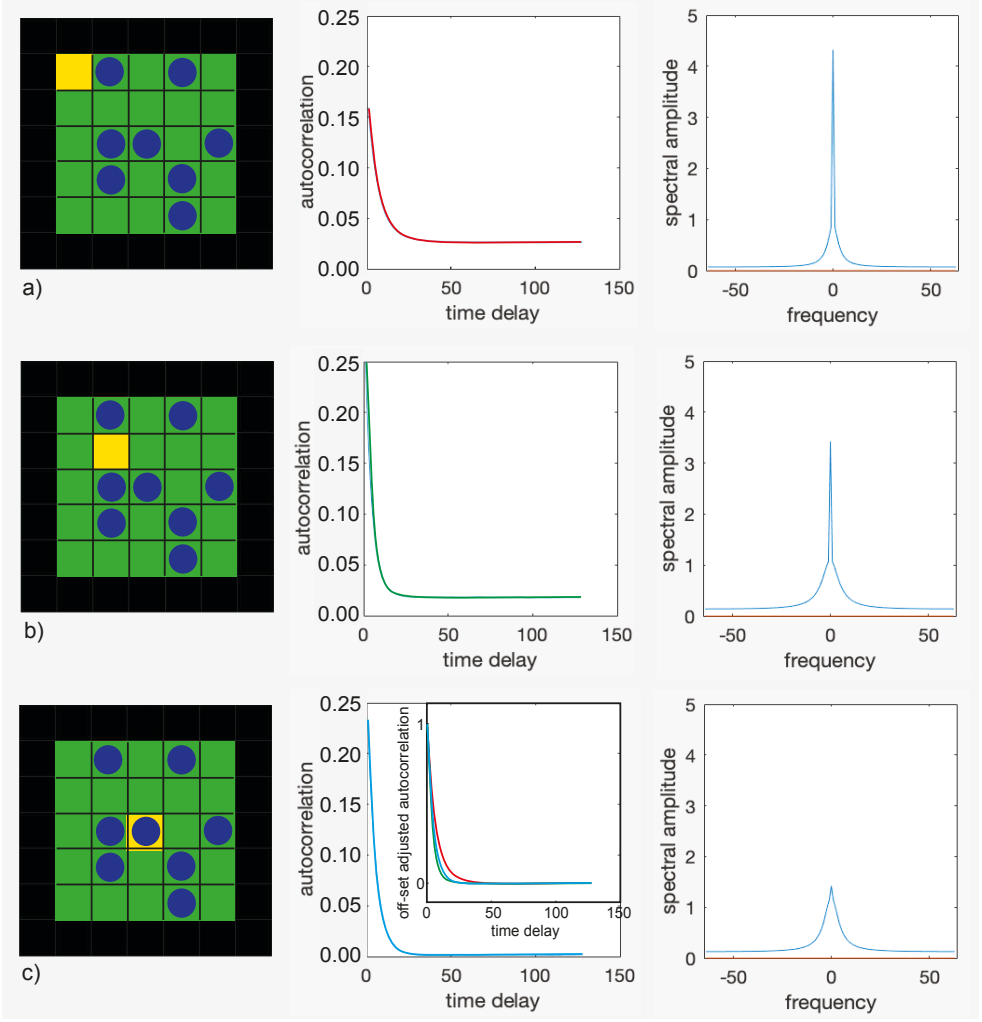


Figure 5. Autocorrelation functions (center) of the occupancy of the yellow cells (left) and the real parts of their Fourier transforms (right) for repulsive interaction at $T$ = 0.1 and $P$ = 0.3. a) Corner cell. b) Off-center cell. c) Center cell. The inset in the middle compares the decays of all three autocorrelation functions after subtraction of the offsets.

While the autocorrelation function is difficult to probe experimentally, the asymmetry parameter $a_{\mathrm{sy}}$, on the other hand, also probes the particle dynamics and

https://doi.org/10.5194/mr-2023-8
Preprint. Discussion started: 22 May 2023


Open Access MAGNETIC RESONANCE Discussions



could be investigated experimentally in a straight-forward manner by relaxation-exchange NMR experiments provided the signal-to-noise ratio is good enough. The parameter depends on the location of the relaxation center in the pore wall (Fig. 6). This dependence has been verified to be identical for all walls of the square pore. Moreover, it exhibits mirror symmetry about the center position (Fig. 6e). For vacancy diffusion in a $5 \times 5$ square pore with walls 7 cells wide (Fig. 6a,b), $a_{\mathrm{sy}}$ varies consistently with position irrespective of the particle interaction being positive, negative or zero but differs strongly in magnitude. It is highest at the corner positions and lowest at the center position. For zero particle interaction, $a_{\mathrm{sy}}$ is more than an order of magnitude smaller than for repulsive interaction, so that the number of particle jumps had to be increased to $10^9$ resulting in 3 h computation time for each data point in the corresponding trace (black) Fig. 6e. Interestingly, $a_{\mathrm{sy}}$ for gas diffusion without particle interaction (green, Fig. 6e) varies in a fashion similar to that for vacancy diffusion, is of magnitude comparable to that of vacancy diffusion (black, Fig, 6e), but does not change sign with position of the active site in the pore wall. In all cases the precision of the asymmetry parameter $a_{\mathrm{sy}}$ obtained in the simulations exceeds the second relevant digit.

The particle dynamics manifested in $a_{\mathrm{sy}}$ are accompanied by variations of the average population density across the pore which is depleted in the first particle layer at the pore wall, enhanced in the next layer, and tapers off towards the pore center in both cases (Figs. 6b,d, Fig. S4). The densities vary in a similar fashion across the pore for both types of diffusion albeit having somewhat different values as can be verified by close inspection of the numbers in each cell in Figs. 6b,d.

The maps in Fig. 6b,d revealing the deviation of local population density from average population density were calculated by summing the 2D maps of particle distributions after each jump, normalizing the resultant maps to the number of jumps and the particle density and subtracting the average mean expected for a constant particle density across all cells in the pore. Further maps of population density variations for the two different pores of Fig. 3 with other sizes and interaction parameters are summarized in Fig. S4 of the supplement. While the particle density varies less with temperature for vacancy diffusion, different density patterns are found at different pressures. The strongest density variations are near the pore wall whether the interaction is repulsive, zero, or attractive, which becomes particularly evident for larger pores (Figs. S4b,d,e). At low density and in the absence of particle interactions

https://doi.org/10.5194/mr-2023-8
Preprint. Discussion started: 22 May 2023


Open Access MAGNETIC RESONANCE Discussions



the main features of the density maps are strikingly similar for vacancy diffusion (Figs. S4b) and gas diffusion (Figs. S4d). The particle density is strongly depleted at the pore corners and near the wall and significantly increased in the next particle layer (Figs. S4e,f). This behavior can be expected in vacancy diffusion when considering, that a jump to an empty pore away from the wall can happen from all directions, while an empty pore at the wall cannot be populated from the side of the wall. Also, for gas diffusion in continuous space, a spherical particle cannot get to the wall closer than half its diameter. For interacting particles, this concentration variation is carried forward in vacancy diffusion with increasing distance from the wall leading to concentration waves which taper off towards the center of the pore and interfere with each other coming from different directions. For small pores interference patterns dominate the density distribution across the pore (Figs. 6b,d and Figs. S4a,c). For noninteracting particles, the decay of the concentration wave towards the pore center is fast with few to no oscillations towards the pore center, while the oscillations are enhanced by thermodynamic interactions between the particles (Fig. S4d, $P = 0.2$). In particular, the population density at the active site in the dent of the complex pore of Fig. 3a depends on the thermodynamic parameters $P$ and $T$ (Figs. S4a,b). It needs to be investigated further how much the NMR relaxation times vary with the position in the standing concentration wave and the associated particle dynamics from the pore wall to the center (Bytchenkoff and Rodts, 2011).

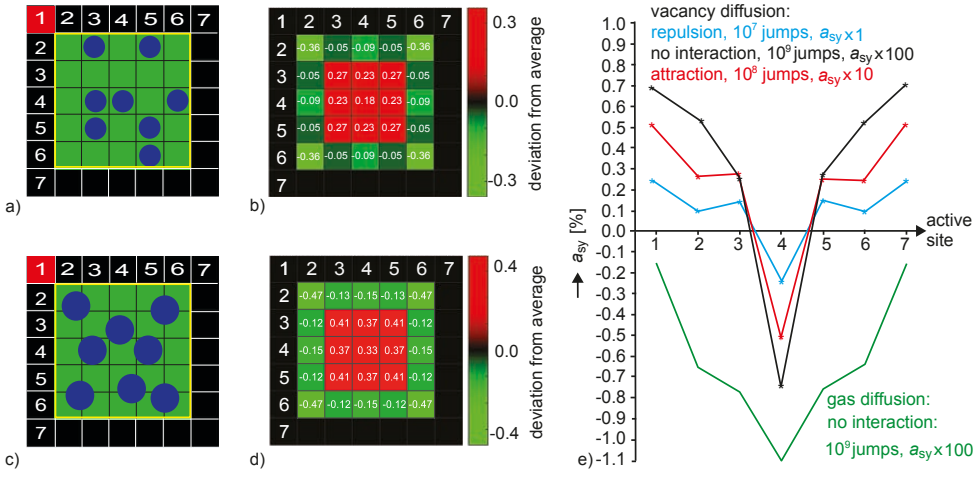


Figure 6. Population density distributions and dependences of the asymmetry parameter $a_{sy}$ on the position of the active relaxation site in the pore wall for $P$ = 0.3 and a pore with 5 × 5 cells. a,b): Vacancy diffusion at $T$ = 0.2 without particle interaction

https://doi.org/10.5194/mr-2023-8
Preprint. Discussion started: 22 May 2023


Open Access MAGNETIC RESONANCE Discussions



as an average over $10^9$ jumps. a) The positions of the relaxation center in the pore wall are numbered from 1 to 7. c,d) Gas diffusion in a square pore with cell walls 5 particle diameters wide. a,c) Schematic drawings of the populated pores. b,d) Deviations of the average population-density distribution from the mean. e) Variations of the asymmetry parameter with the position of the active site in the cell wall for differently interacting particles for vacancy and for gas diffusion. The mirror symmetry for each trace confirms the sufficient precision of the simulation.

## 4. Discussion

For two-dimensional vacancy diffusion, jumps of randomly selected particles from one cell to an empty neighbor cell and for two-dimensional gas diffusion with variable paths between collisions in model pores give rise to asymmetry in the exchange statistics between three sites depending on temperature and pressure. The two pore geometries were investigated, one modeling a section of a porous solid grain particle (cf. supplementary information) and the other being a small square pore with an active site, e. g. a catalytically active center. The interaction between the particles as well as the particles and the walls are identical in the reported data but can be repulsive, zero, or attractive in the vacancy-diffusion case while it is zero for the gas-diffusion case. The observed asymmetry parameters vary in a range on the order of $-1\% < a_{\mathrm{sy}} < 1\%$, i. e., up to 1% of all particles in the pore may not follow detailed balance between all pairs of sites but move coherently in circles between the three sites. It is emphasized that this circular exchange is between the pools of particles representing the three sites, and it is not a motion followed by individual particles completing circular jumps. If the free interaction energy is set to zero in the vacancy-diffusion simulations, the magnitude of the observed asymmetry $a_{\mathrm{sy}}$ is smaller than $0.01\%$ (Fig. 4c,f), a value which could only be observed at $10^9$ jumps of 7 particles in the pore for vacancy as well as gas diffusion (Fig. 6e). Given positive or negative interaction energies, the variations of $a_{\mathrm{sy}}$ with temperature $T$ appear rapid, reminiscent of phase transitions (Figs. 4a Figs. S3a). The variations of $a_{\mathrm{sy}}$ with pressure corresponding to population density $P$ are smooth (Figs. 4b, Figs. S3b). Either positive or negative values of $a_{\mathrm{sy}}$ are observed as $T$ or $P$ change. A sign change of $a_{\mathrm{sy}}$ reports a change in the sense of the circular exchange (cf. Fig. 1).

For a simple square pore, the asymmetry parameter varies with the position of the active site in the cell wall, exhibiting mirror symmetry with respect to the wall center (Fig. 6e). Moreover, the autocorrelations functions and their Fourier transforms have been determined for the occupancy time tracks of selected cells at specific positions

https://doi.org/10.5194/mr-2023-8
Preprint. Discussion started: 22 May 2023


Open Access MAGNETIC RESONANCE Discussions



inside a small square pore for $10^7$ jumps of all particles in the pore (Fig. 5). The track function had been devised to have zero mean for the average cell population. Depending on the position of the cell inside the pore, the autocorrelations functions and their Fourier transforms vary. Specifically, the autocorrelation function can exhibit a significant constant offset. At these positions inside the pore, the particle densities are different from the pore average, and the cell is on average more empty or occupied than expected if the exchange between all cells were the same. This conclusion is supported by the observed deviations of the cell occupancies from the pore average (Figs. 6b,d, Fig. S4). Near the pore wall the average population density is depleted and varies in an oscillatory manner along the pore wall. Further towards the center of the pore the average population density increases sharply and then tapers off towards the pore center to a value slightly above the average density.

The observations for vacancy diffusion in a square pore with $5 \times 5$ cells are compared to independent simulations of gas diffusion of non-interacting particles in a square pore with an edge length of 5 particle diameters also allowing 7 relaxation centers along the pore wall (Figs. 6a,c). A similar variation of the asymmetry parameter is found as for vacancy diffusion, but the asymmetry parameter is negative for all positions of the active site (Fig. 6e). Moreover, the depletion of the average particle density at the pore wall and its subsequent variation towards the center are similar with the exception, that oscillations of the average particle density along the pore wall are weaker for gas diffusion at short observation intervals (Figs. 6b,d) but increase with the duration of the observation intervals (Fig. S5). The lack of a sign change in the asymmetry parameter with changing position of the active site may be explained by destructive interference of particle collisions from multiple sites with the wall within one discrete particle diameter and the fact, that the free path length between collisions in gas diffusion is not limited to the next cell as in vacancy diffusion but can range up to the pore diameter.

Taken together, the observed asymmetry in the three-site exchange and the variation of the jump statistics with position inside the pore point at diffusive resonance phenomena like standing waves of air in pipes as reported by Kundt (Kundt, 1866) or of vibrating plates as reported by Chladni (Chladni, 1787). Stochastic resonance phenomena have been observed with NMR first by Sleator, Hahn et al. (Sleator et al., 1985) and subsequently studied in detail by Müller, Jerschow, et al. in different scenarios (Müller and Jerschow, 2005; Schlagnitweit and Müller, 2012). In NMR, the

https://doi.org/10.5194/mr-2023-8
Preprint. Discussion started: 22 May 2023


Open Access MAGNETIC RESONANCE Discussions



magnetization fluctuating with the thermal motion of the nuclear spins assumes the role of the particles and the resonance circuit assumes the role of the pore.

Three-site exchange can be viewed as a finite difference approximation to the Laplace operator (van Kampen, 1992; Kuprov, 2022) governing Fick's second law (Fick, 1855). Considering some local site *N* with neighbor sites *N*-1 and *N*+1 right and left, the mass flow to and from site *N* given by eqn. (1) is

$$\frac{\mathrm{d}m_N(t)}{\mathrm{d}t} = k_{N,N-1}m_{N-1} - k_{N-1,N}m_N + k_{N,N+1}m_{N+1} - k_{N+1,N}m_N, \tag{10}$$

Taking the limit to infinitesimal small distance $\Delta r \to \partial r$ between the neighboring sites leads to $k_{j,i} = k$, demonstrating that (10) is a finite difference approximation of a second spatial derivative balanced by the temporal variations of $m$ during infinitesimal time $\partial t$,

$$(k\, m_{N-1} - 2\, k\, m_N + k\, m_{N+1})/\Delta r^2 \approx k\frac{\mathrm{d}^2 m}{\mathrm{d}^2 r^2} = \frac{\mathrm{d}m}{\mathrm{d}t}/\Delta r^2. \tag{11}$$

In this limit, eqn. (11) becomes Fick's second law with the diffusion coefficient $D = k\Delta r^2$. This back-of-the-envelope argument indicates that the observed asymmetry of three-site exchange is a property of Fick's second law.

The diffusion equation applicable to longitudinal magnetization in NMR instead of particle masses $m$ is the Bloch-Torrey equation (Torrey, 1956),

$$\frac{\partial}{\partial t}m(\boldsymbol{r},t) = D\boldsymbol{\nabla}^2 m(\boldsymbol{r},t) - \mu\, m(\boldsymbol{r},t), \tag{12}$$

where $m$ now is the magnetization deviation from thermal equilibrium and $\mu$ is the bulk relaxation rate. $m(\boldsymbol{r},t)$ solves this equation in terms of an expansion into normalized eigenfunctions $\phi_n(\boldsymbol{r})$ with amplitudes $A_n$ and eigenvalues $\tau_n$ (Brownstein and Tarr, 1977; Song, 2000)

$$m(\boldsymbol{r},t) = e^{-\mu t}\sum_{n=0}^{\infty} A_n\, \phi_n(\boldsymbol{r})\, e^{-\frac{t}{\tau_n}}. \tag{13}$$

The eigenvalues are determined by the boundary condition

$$D\, \boldsymbol{n}\, \boldsymbol{\nabla}\phi_n(\boldsymbol{r}) = \rho\, \phi_n(\boldsymbol{r}), \tag{14}$$

where $\rho$ is the surface relaxivity and $\boldsymbol{n}$ is the unit vector normal to the surface. The lowest normal mode $\phi_0$ has no nodes. The higher normal modes $\phi_n$ possess nodal surfaces. The higher diffusion eigenmodes have been detected by NMR with selective excitation of partial pore volumes making use of field gradients internal to the pore (Song, 2000). These experimental results reported by Song agree with the Monte Carlo simulations of diffusive translational motion in pores reported here, in that the population density varies across the pore and that the offset of the autocorrelation function of the local pore occupancy depends on the position of the cell in the pore.

https://doi.org/10.5194/mr-2023-8
Preprint. Discussion started: 22 May 2023


Open Access MAGNETIC RESONANCE Discussions



From the exchange asymmetry of the particles in the square pore investigated in Fig. 6 (Fig. 7) a suggestive picture emerges for confined vacancy diffusion, where the diffusion lengths are confined to the distances from the particle to the direct neighbor cells. Depending on the sign of the asymmetry parameter (Fig. 7a), a small fraction of the particles (blue circles) prefers the direct path towards or away from the active site (red square) at the pore boundary over the path along the boundary to or from the active site. In the center of the wall, the direct path away from the active site to the bulk is preferred over the path along the pore wall when leaving the contact region with the active site (Fig. 7b). But because jumps are allowed in vacancy diffusion only to neighboring cells, the cells 2 at the wall right and left of the active site 3 must be populated from the bulk 1 by direct jumps form the bulk to the wall. For these jumps, the asymmetry parameter is positive, as observed for the off-center positions of the active site (Fig. 6e). Given the symmetry of the square pore, the in-plane translational diffusion paths resulting from the variation of the asymmetry parameters with the position of the active site on the pore wall (Fig. 6e) demand the existence of eight diffusion vortices inside the pore (Fig. 7d). The symmetry of this in-plane translational diffusion pattern matches the symmetry of one of the node patterns of the out-of-plane vibrational modes of a square plate observed by Chladni (Fig. 7e) about a quarter of a millennium earlier (Chladni, 1787). This suggests that the dynamic of vacancy diffusion observed in the computer model reported here is a resonance feature of the pore and thus an eigenmode of pore diffusion. This resonance effect is far less pronounced for gas diffusion (Fig. 7c) where the free paths between collisions can span the entire cell. Because the mass flow from relaxation site 2 to the active site 3 can be sustained from any position at the pore wall the asymmetry parameter does not need to change sign when the active site moves along the pore wall (Fig. 7e), and the circular paths can have various shapes and can extend across the entire pore, so that the vortex pattern is largely washed out.

Given the technological importance of fluid motion in small pores in heterogeneous catalysis (Kärger et al., 2012), it will be interesting to explore, if correlated motion resulting from standing particle-concentration wave patterns near pore walls can be enhanced by external drivers like ultrasound, electric or magnetic fields. The standing waves could be enhanced by tuning the driver frequency to the pore resonance like a musician enforces resonance modes on a musical instrument when playing. To enhance the diffusion eigenmodes, also low-power broad-band,

https://doi.org/10.5194/mr-2023-8
Preprint. Discussion started: 22 May 2023


Open Access MAGNETIC RESONANCE Discussions



forced oscillations can be considered such as in Fourier transform infrared spectroscopy (Michelson, 1903) and stochastic NMR spectroscopy (Ernst, 1970), while triggering free oscillations by high-power impulses may destroy the porous medium under study.

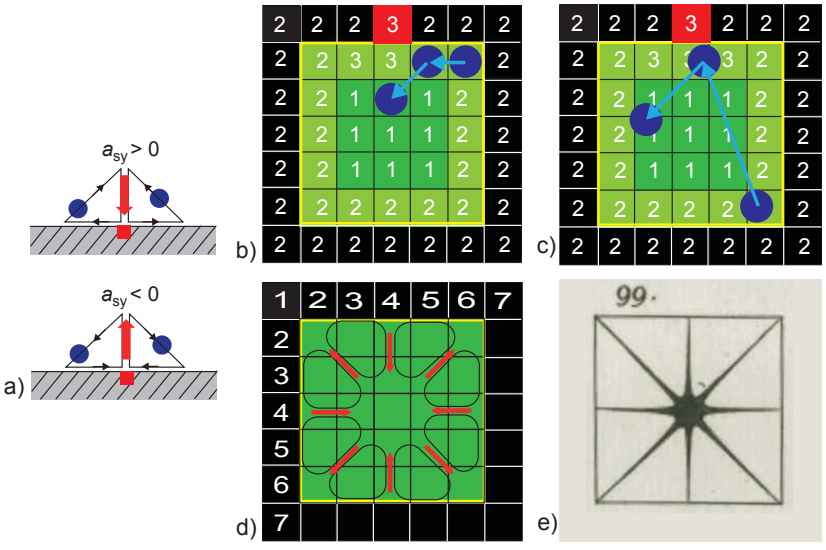


Figure 7. Illustration of the exchange asymmetry for the square pore of Fig. 6a. a) Depending on the sign of the asymmetry parameter, a small fraction of diffusing particles (blue circles) prefers the direct path towards or away from the active site (red square) at the pore boundary over the path along the boundary from the active site. b) Vacancy diffusion for negative asymmetry parameter and the active site 3 in the center of the pore wall. Jumps are limited to the next nearest cells. The direct path away from the active site to the bulk 1 in the center is preferred over the path along the pore wall 2 when leaving the contact region with the active site. c) Gas diffusion for negative asymmetry parameter and the active site 3 in the center of the pore wall. The free paths between collisions can span the entire cell. d) In-plane translational diffusion paths resulting from the variation of the asymmetry parameters with the position of the active site on the pore wall depicted in Fig. 6e. e) Out-of-plane vibrational mode of a square plate observed by Chladni (Chladni, 1787).

## 5. Summary

The evidence provided by molecular dynamics simulations of random particle jumps on a 2D checkerboard and by simulations of 2D gas diffusion with topological confinements supports the notion, that asymmetry in three-site exchange maps reports the non-Brownian diffusion dynamics of confined particles. Depending on the sign of the asymmetry parameter, for a small fraction of diffusing particles, the direct path

https://doi.org/10.5194/mr-2023-8
Preprint. Discussion started: 22 May 2023


Open Access MAGNETIC RESONANCE Discussions



568 towards or away from the active site at the pore boundary is preferred over the path
569 along the boundary to or from the active site (Fig. 7). Both, vacancy diffusion and gas
570 diffusion produce congruent results. Yet, the reported simulations are limited to two
571 dimensions, and it may be argued that the asymmetry of exchange vanishes in the
572 more common pores with three spatial dimensions. But two-dimensional diffusion is
573 not an abstract model and arises for gas atoms adsorbed to metal surfaces (Oura et
574 al., 2013), so that the coherent particle diffusion indicated by the non-zero asymmetry
575 parameter may be observed there. Meanwhile experiments are in progress (Fricke and
576 Reimer, 2022) investigating three-site particle exchange in different systems including
577 highly regular pore structures such as molecular organic frameworks (Stallmach et al.,
578 2006; Forse et al., 2020). Moreover, future work aims at expanding the current models
579 of vacancy and gas diffusion to three dimensions and different types of interactions
580 between neighbor particles and walls to gain further insight into the details of local
581 particle concentrations and thermodynamic equilibrium fluxes inside pores. But given
582 the congruent simulation evidence for vacancy diffusion and gas diffusion in two-
583 dimensional confinements it is concluded, that confined diffusion is not fully random
584 but exhibits local concentration gradients that can lead to flux anomality violating the
585 principle of detailed balance. Especially, Boltzmann's claim, that "The walls do not
586 interfere, because the molecules are reflected from them like elastic balls; that is,
587 recede from them just like that, as if the space beyond the walls would be filled with
588 similarly conditioned gas" is not fulfilled for small pores as evidenced by the observed
589 population-density variations across pores and the known existence of diffusion
590 eigenmodes. Accordingly, the principle of detailed balance does not apply to a fraction
591 of particles close to the pore wall. On a rigorous absolute scale, this means that
592 apparently random motion in phase-separated environments is not fully random and
593 time reversal does not apply to all particles. Since we live in a phase-separated
594 universe, Einstein may be right after all when he wrote to Bohr on 14 December 1926
595 (Born, 1959): "Die Quantenmechanik ist sehr achtunggebietend. Aber eine innere
596 Stimme sagt mir, daß das noch nicht der wahre Jakob ist. Die Theorie liefert viel, aber
597 dem Geheimnis des Alten bringt sie uns kaum näher. Jedenfalls bin ich überzeugt, daß
598 der nicht würfelt." This statement is commonly paraphrased by "God does not play
599 dice". It may be interesting to find out, what role diffusion eigenmodes at interfaces
600 between different states of matter played accumulated over billions of years in the
601 evolution of live in the universe.

https://doi.org/10.5194/mr-2023-8
Preprint. Discussion started: 22 May 2023


Open Access MAGNETIC RESONANCE Discussions



## Author Contributions

BB posed the question, executed the simulations of confined vacancy diffusion, and wrote the manuscript. MA worked out the algorithm for vacancy diffusion along with BB and supervised MP. MP programmed the algorithm for confined gas diffusion and executed the gas-diffusion simulations.

## Acknowledgement

BB thanks Thomas Wiegand at RWTH Aachen University for stimulating discussions, hosting him as a PostProf, and access to the computing facilities. He also thanks Ilya Kuprov for his flash of inspiration on linking three-site exchange to Fick's second law at a random EUROMAR 2022 breakfast encounter and Stephan Appelt, Gerd Buntkowsky, and Jeffrey Reimer for stimulating discussions. Special thanks go to the unknown reviewer who commented on the manuscript (Gao and Blümich, 2020), that asymmetry in three-site exchange violates the principle of detailed balance.

## Code availability

The codes for simulating confined 2D vacancy diffusion and confined 2D gas diffusion is available from the authors upon request.

## Conflict of Interest statement

Other than that BB is on the advisory board of Magnetic Resonance the authors declare no conflict of interest.

## References

Bialynicki-Birula, I. and Bailynicky-Birula, I., Modeling Reality, Oxford University Press, Oxford, 2004.

Björgvinsdóttir, S., Moutzouri, P., Walder, B. J., Matthey, N., and Emsley, L., Hyperpolarization transfer pathways in inorganic materials, J. Magn. Reson. 323, 106888, 2021.

Born, M., Physik im Wandel meiner Zeit, 3rd ed., Vieweg & Sohn, Braunschweig, 1959.

Brownstein, K.R. and Tarr, C. E., Spin-Lattice Relaxation in a System Governed by Diffusion, J. Magn. Reson. 26, 17–24, 1977.

https://doi.org/10.5194/mr-2023-8
Preprint. Discussion started: 22 May 2023


Open Access MAGNETIC RESONANCE Discussions



635 Bunde, A., Caro, J., Kärger, J., and G. Vogel, eds., Diffusive Spreading in Nature and
636 Technology, Springer Nature, Cham, 2018.
637 Bytchenkoff, D., and Rodts, S., Structure of the two-dimensional relaxation spectra
638 seen within the eigenmode perturbation theory and the two-site exchange model, J.
639 Magn. Reson. 208, 4–19, 2011.
640 Callaghan, P. T. and Stepisnik, J., Modulated Gradient NMR, J. Magn. Reson. 117,
641 118–122 (1995).
642 Callaghan, P.T., Translational Dynamics and Magnetic Resonance: Principles of
643 Pulsed Gradient Spin Echo NMR, Oxford University Press, Oxford, 2011.
644 Chladni, E. F. F., Entdeckungen über die Theorie des Klanges, Leipzig, Weidmanns
645 Erben und Reich, 1787.
646 Einstein, A., Zur Quantentheorie der Strahlung, Physikalische Zeitschrift 18, 121–128,
647 1917.
648 Ernst, R. R., Bodenhausen, G., and Wokaun, A., Principles of Nuclear Magnetic
649 Resonance in One and Two Dimensions, ClarendonPress, Oxford, 1987.
650 Ernst, R. R., Magnetic Resonance with Stochastic Excitation, J. Magn. Res. 3, 10–27,
651 1970.
652 Feynman, R., Leighton, R. B., and Sands, M., The Feynman Lectures on Physics, vol.
653 1, chapter 46, Addison-Wesley, Reading, Fourth Printing, 1966
654 Fick, A., Ueber Diffusion, Annalen der Physik 94, 59–86, 1855.
655 Forse, A. C., Colwell, K. A., Gonzalez, M. I., Benders, S., Torres-Gavosto, R. M.,
656 Blümich, B., Reimer, J. A., and Long, J. R., Influence of Pore Size on Carbon Dioxide
657 Diffusion in Two Isoreticular Metal–Organic Frameworks, Chem. Mat. 32, 3570–3576,
658 2020.
659 Fricke, S. and Reimer J., personal communication, 2022.
660 Gao, Y., and Blümich, B., Analysis of three-site $T_2$-$T_2$ exchange NMR, J. Magn. Reson.
661 315, 106740, 2020.
662 Grebenkov, D. S., A fast random walk algorithm for computing the pulsed-gradient
663 spin-echo signal in multiscale porous media, J. Magn. Reson. 208, 243–255, 2011.
664 Hughes, B. D., Random Walks and Random Environments, Clarendon Press, Oxford,
665 1995.
666 Jeener, J., Meier, B. H., Bachmann, P., and Ernst, R. R., Investigation of exchange
667 processes by two-dimensional NMR spectroscopy, J. Chem. Phys. 71 4546–4553,
668 1979.

https://doi.org/10.5194/mr-2023-8
Preprint. Discussion started: 22 May 2023


Open Access MAGNETIC RESONANCE Discussions



669 Kärger, J., Ruthven, D. M., and Theodorou, D. N., eds., Diffusion in Nanoporous
670 Materials, vol. 1, Wiley-VCH, Weinheim, 2012.
671 Kundt, A., Über eine neue Art akustischer Staubfiguren und über die Anwendung
672 derselben zur Bestimmung der Schallgeschwindigkeit in festen Körpern und Gasen,
673 Annal. Phys. Chem. 203, 497–523, 1866.
674 Kuprov, I., private communication with BB at the EUROMAR 2022 conference in
675 Utrecht, July 10–14, 2022.
676 L. Boltzmann, Weitere Studien über das Wärmegleichgewicht unter Gasmolekülen,
677 Sitzungsber. Kais. Akad. Wiss., Wien, Math, Natruwiss. Classe 66, 275-370, 1872.
678 Lacabanne, D., Wiegand, T., Di Cesare, M., Orelle, C., Ernst, M., Jault, J.-M., Meier,
679 B.H., and Böckmann, A., Solid-State NMR Reveals Asymmetric ATP Hydrolysis in the
680 Multidrug ABC Transporter BmrA, J. Am. Chem. Soc. 144, 12431–12442, 2022.
681 Lee, J.-H., Labadie, C., Springer Jr., C. S., and Harbison G.S., Two-Dimensional
682 Inverse Laplace Transform NMR: Altered Relaxation Times Allow Detection of
683 Exchange Correlation, J. Am. Chem. Soc. 115, 7761–7764, 1993.
684 Maxwell, J. C., On the dynamical theory of gases, Philos. Trans. R. Soc. London 157
685 49–88, 1867.
686 McDonald, P. J., Korb, J.-P., Mitchell, J., and Monteilhet, L., Surface relaxation and
687 chemical exchange in hydrating cement pastes: A two-dimensional NMR relaxation
688 study, Phys. Rev. E 72, 011409, 2005.
689 Michelson, A. A., Light Waves and Their Uses, The University of Chicago Press,
690 Chicago, 1903.
691 Müller, N. and Jerschow, A., Nuclear Spin Noise Imaging, PNAS 103, 6790–6792,
692 2005.
693 Olaru, A. M., Kowalski, J., Sethi, V., and Blümich, B., Exchange relaxometry of flow at
694 small Péclet numbers in a glass bead pack, J. Magn. Reson. 220, 32–44, 2012.
695 Oura, K., Lifshits, V. G., Saranin, A. A., Zotov, A. V., and Katayama, M., Surface
696 Science: An Introduction, Springer, Berlin, 2013, chapter 13.
697 Parsons, E. C., Does, M. D., and Gore J.C., Temporal Diffusion Spectroscopy: Theory
698 and Implementation in Restricted Systems Using Oscillating Gradients, Magn. Reson.
699 Med. 55, 75–84, 2006.
700 Sabelfeld, K. K., Monte Carlo Methods in Boundary Value Problems, Springer-Verlag,
701 Berlin, 1991.
702 Sandstrom, J., Dynamic NMR Spectroscopy, Academic Press, Cambridge, MA, 1983

https://doi.org/10.5194/mr-2023-8
Preprint. Discussion started: 22 May 2023


Open Access MAGNETIC RESONANCE Discussions



703 Schlagnitweit, J. and Müller, N., The first observation of Carbon-13 spin noise spectra,
704 J.Magn. Reson. 224, 78–81, 2012.
705 Seitz, F., On the Theory of Vacancy Diffusion in Alloys, Phys. Rev. 74, 1513–1523,
706 1948.
707 Sleator, T., Hahn, E.L., Hilbert, C., and Clarke, J., Nuclear Spin Noise, Phys. Rev. Lett.
708 55, 1742–1745, 1985.
709 Song, Y. Q., Detection of the High Eigenmodes of Spin Diffusion in Porous Media,
710 Phys. Rev. Lett 85, 3887-3881, 2000.
711 Stallmach, F., Glöggler, S., Künzel, V., Kärger, J., Yaghi, O. M., Hesse, M., and Müller,
712 U., NMR Studies on the Diffusion of Hydrocarbons on the Metal-Organic Framework
713 Material MOF-5, Angew. Chem. In. Ed. 45, 2123–2126, 2006.
714 Stepišnik, J., Mohoric, A., Lahajnar, G., Mattea, C., Stapf, S., and Sersa, I., Velocity
715 autocorrelation spectra in molten polymers measured by NMR modulated gradient
716 spin-echo, Europhysics Lett. 106, 27007, 2014.
717 Torrey, H. C., Bloch Equations with Diffusion Terms, Phys. Rev. 104, 563–565, 1956.
718 Valiullin, R., ed., Diffusion NMR of Confined Systems, R. Soc. Chem., Cambridge,
719 2017.
720 van Kampen, N. G., Stochastic Processes in Physics and Chemistry, Elsevier,
721 Amsterdam, 1992.
722 Van Landeghem, M., Haber, A., d'Espinose de Lacaillerie J.-B., and Blümich, B.,
723 Analysis of Multisite 2D Relaxation Exchange NMR, Concepts Magn. Reson. 36A,
724 153–169, 2010.
725 Wolf-Gladrow, D. A., Lattice-Gas Cellular Automata and Lattice Boltzmann Models,
726 Springer, Berlin, 2000.
727